

1 **Multiple pathways for the formation of secondary organic aerosol in North China Plain**
2 **in summer**

3 Yifang Gu^{1,3}, Ru-Jin Huang^{1,2,3}, Jing Duan¹, Wei Xu¹, Chunshui Lin¹, Haobin Zhong^{1,3}, Ying
4 Wang¹, Haiyan Ni¹, Quan Liu⁴, Ruiguang Xu^{5,6}, Litao Wang^{5,6}, Yong Jie Li⁷

5 ¹SKLLQG, Center for Excellence in Quaternary Science and Global Change, Institute of Earth
6 Environment, Chinese Academy of Sciences, Xi'an 710061, China

7 ²Institute of Global Environmental Change, Xi'an Jiaotong University, Xi'an 710049, China

8 ³University of Chinese Academy of Sciences, Beijing 100049, China

9 ⁴State Key Laboratory of Severe Weather & Key Laboratory of Atmospheric Chemistry of C
10 MA, Chinese Academy of Meteorological Sciences, Beijing 100081, China

11 ⁵Department of Environmental Engineering, School of Energy and Environmental Engineering,
12 Hebei University of Engineering, Handan 056038, China

13 ⁶Hebei Key Laboratory of Air Pollution Cause and Impact, Handan 056038, China

14 ⁷Department of Civil and Environmental Engineering, and Centre for Regional Oceans, Faculty
15 of Science and Technology, University of Macau, Taipa, Macau 999078, China

16 *Correspondence to:* Ru-Jin Huang (rujin.huang@ieecas.cn)

17

18

19 **Abstract**

20 Secondary organic aerosol (SOA) has been identified as a major contributor to fine
21 particulate matter (PM_{2.5}) in North China Plain (NCP). However, the chemical mechanisms
22 involved are still unclear due to incomplete understanding of its multiple formation processes.
23 Here we report field observations in summer in Handan of NCP, based on high-resolution
24 online measurements. Our results reveal the formation of SOA via photochemistry and two
25 types of aqueous-phase chemistry, the latter of which include nocturnal and daytime processing.
26 The photochemical pathway is the most important under high O_x (=O₃ + NO₂) conditions (65.1
27 ± 20.4 ppb). The efficient SOA formation from photochemistry (O_x-initiated-SOA) dominated
28 the daytime (65% to OA) with an average growth rate of 0.8 μg m⁻³ h⁻¹. During the high relative
29 humidity (RH: 83.7 ± 12.5 %) period, strong nocturnal aqueous-phase SOA formation (aq-SOA)
30 played a significant role in SOA production (45% to OA) with a nighttime growth rate of 0.6
31 μg m⁻³ h⁻¹. Meanwhile, an equally fast growth rate of 0.6 μg m⁻³ h⁻¹ of O_x-initiated-SOA from
32 daytime aqueous-phase photochemistry was also observed, which contributed 39% to OA,
33 showing that photochemistry in the aqueous phase is also a non-negligible pathway in summer.
34 The primary-related-SOA (SOA attributed to primary particulate organics) and aq-SOA are
35 related to residential coal combustion activities, supported by distinct fragments from
36 polycyclic aromatic hydrocarbons (PAHs). Moreover, the conversion and rapid oxidation of
37 primary-related-SOA to aq-SOA could be possible in the aqueous phase under high-RH
38 conditions. This work sheds light on the multiple formation pathways of SOA in ambient air of
39 complex pollution, and improves our understanding of ambient SOA formation and aging in
40 summer with high oxidation capacity.

41

42 **KEYWORDS:** secondary organic aerosol, aqueous-phase chemistry, photochemistry, multiple-
43 phase chemistry, complex air pollution

44

45 1. Introduction

46 Rapid economic growth and urbanization processes have led to severe particulate air
47 pollution in China, affecting air quality, climates and human health (Huang et al., 2014;
48 Cohen et al., 2017; An et al., 2019). Organic aerosol (OA) is a major component of aerosol
49 particles, consisting of 20-90% of fine particle mass (Jimenez et al., 2009; Zhang et al., 2011).
50 OA is either emitted directly from primary sources (referred to as primary OA, POA) such as
51 traffic, cooking, coal combustion, and biomass burning, or produced through gas-to-particle
52 conversion (referred to as secondary OA, SOA) in the atmosphere. In recent years, with the
53 implementation of control measures, the POA fraction is decreasing and SOA fraction is
54 increasing in North China Plain (NCP), indicating that SOA is becoming more critical for urban
55 air quality (Huang et al., 2019; Xu et al., 2019; Gu et al., 2020). However, our understanding
56 of the formation mechanisms and evolution processes of SOA is still limited.

57 Generally, SOA can be formed through gas-phase photochemical oxidation of volatile
58 organic compounds (VOCs) followed by nucleation or condensation of oxidation products onto
59 the preexisting particles (Donahue et al., 2006). Herndon et al., (2008) showed that oxygenated
60 organic aerosol (OOA), a surrogate of SOA, was well correlated with odd oxygen ($O_x = O_3 +$
61 nitrogen dioxide (NO_2)) during photochemical processing. SOA can also be formed in the
62 aqueous phase on wet aerosols, clouds and fogs through further chemical processes of water-
63 soluble organic compounds or organic products of gas-phase photochemistry (Ervens et al.,
64 2011, 2014). A growing number of laboratory studies and field measurements have indicated
65 that aqueous-phase processes contribute efficiently to the formation of SOA (Gilardoni et al.,
66 2016; Bikkina et al., 2017). However, how photochemistry and aqueous-phase chemistry
67 coordinate to affect the formation of SOA is still unclear, despite numerous measurements to
68 explore this question using aerosol chemical speciation monitor (ACSM) or aerosol mass
69 spectrometer (AMS) (Hu et al., 2016b; Hu et al., 2017; Sun et al., 2016; Li et al., 2017; Sun et
70 al., 2018b; Huang et al., 2019; Gu et al. 2020; Kuang et al., 2020). Field measurements in
71 Beijing suggested that gas-phase photochemical oxidation can play a dominant role in SOA
72 formation (Sun et al., 2016; Hu et al., 2016a). Xu et al., (2017) showed that less oxidized-OOA
73 (LO-OOA) was mainly formed through photochemical oxidation, while the more oxidized-
74 OOA (MO-OOA) formation was dominantly formed by aqueous-phase chemistry in Beijing
75 for different seasons. Kuang et al. (2020) investigated the effects of gas-phase and aqueous-
76 phase photochemical processes on the formation of SOA and found that photochemical
77 aqueous-phase SOA formation dominantly contributed to daytime OOA formation in winter
78 Gucheng, located between Beijing (~100 km) and Baoding (~40 km) on the NCP. We found
79 that photochemical processing attributed mostly to MO-OOA in summertime Beijing (Gu et al.,
80 2020). Although these studies provided important insights into SOA formation processes, our
81 understanding on the photochemical and aqueous-phase formation pathways for SOA and their

82 impacts on oxidation degree are far from complete. This lack of understanding is especially so
83 under the conditions that atmospheric oxidative capacity and pollution characteristics have been
84 largely changing in China due to large reduction in direct emissions of air pollutants.

85 In this study, we investigated the photochemical versus aqueous-phase processing for SOA
86 composition and oxidation degree of OA in summertime Handan, which is a typical
87 industrialized city in the NCP region. The city is located at the intersectional area of Hebei,
88 Shanxi, Henan, and Shandong—four heavily urbanized and industrialized provinces (Fig. S1),
89 and it is therefore an ideal site to investigate the SOA formation pathways in the NCP region.
90 The multiple formation pathways, evolution of SOA composition, and oxidation degree under
91 different meteorological conditions were discussed, which sheds light on the aqueous-phase
92 chemistry and photochemical processing in SOA formation in the NCP region of China.

93 **2. Experimental methods**

94 **2.1 Sampling site**

95 Measurements were conducted from 10th August 2019 to 17th September 2019 on the campus
96 of Hebei University of Engineering (36.57 N, 114.50 E), located at the southeast edge of urban
97 Handan (Fig. S1). The site is surrounded by a school and residential areas, ~300 m north to
98 South Ring Road and ~400 m northeast to the Handan Highway (S313). The sampling site is
99 on the rooftop of a four-floor building, approximately 12 m above the ground.

100 **2.2 Instrumentation**

101 Real-time non-refractory PM_{2.5} composition was measured by a soot particle long time-of-
102 flight aerosol mass spectrometer (SP-LToF-AMS, Aerodyne Research Inc.) with a time
103 resolution of 1 min. The detailed instrument description and operation of AMS were reported
104 in Onasch et al., (2012). Compared to the conventional AMS, the LToF mass analyzer can
105 provide much better mass resolution of ~8000. During the campaign, the instrument was
106 operated in the “laser off” mode and only the standard tungsten vaporizer was applied.
107 Therefore, only non-refractory PM_{2.5} components (NR-PM_{2.5}) were measured, including
108 organics (Org), nitrate (NO₃), sulfate (SO₄), ammonium (NH₄), and chloride (Chl). Ambient
109 air was sampled and dried by a Nafion dryer (MD-700-24S, Perma Pure, Inc.) at a flow rate of
110 5 L min⁻¹, and then sub-sampled into the SP-LToF-AMS at a flow rate of ~ 0.1 L min⁻¹. An
111 aerodynamic PM_{2.5} lens was used to focus the particle into a beam, which was then impacted
112 on the heated tungsten surface (~ 600 °C) and flash-vaporized. Electron ionization with 70 eV
113 was used to ionize the vaporized gases. The ionization efficiency (IE) and the relative ionization
114 efficiency (RIE) calibrations (Jimenez et al., 2003) were conducted by using 350 nm
115 ammonium nitrate (NH₄NO₃) and ammonium sulfate ((NH₄)₂SO₄) particles.

116 Gaseous pollutants including SO₂ (9850 SO₂ analyzer, Ecotech), NO₂ (Model 42i NO-NO₂-
117 NO_x analyzer, Thermo Scientific), CO (Model 48i carbon monoxide analyzer, Thermo
118 Scientific), O₃ (Model 49i ozone analyzer, Thermo Scientific), and meteorological parameters
119 including RH and temperature were also measured during the observation period. Furthermore,
120 an aethalometer (Model AE-33, Magee Scientific) was deployed to measure the mass
121 concentration of black carbon (BC) at a time resolution of 1 min.

122 **2.3 Data Analysis**

123 The data analysis software (SQUIRREL, version 1.63I and PIKA, 1.23I) within Igor Pro 6.37
124 (WaveMetrics) was used to analyze the AMS data. The experimental RIE values of 4 (NH₄)
125 and 1.2 (SO₄) and the standard RIE values of 1.4 (Org), 1.1 (NO₃) and 1.3 (Chl) were used.
126 The composition-dependent collection efficiency (CDCE, Middlebrook et al., 2012) was used
127 to compensate for the incomplete detection caused by particle bounce on the vaporizer. An
128 improved Ambient (I-A) method was adopted for the elemental ratio analysis of high-resolution
129 (HR) OA mass spectra, such as oxygen-to-carbon (O:C), and hydrogen-to-carbon (H:C) ratios
130 (Canagaratna et al., 2015), which reflect the relative composition and oxidation degree for
131 different OA source. In our study, PMF was performed on HR mass spectra of OA for ions with
132 m/z values of 12-120, together with the signals from integer m/z values between 121 to 300 (i.e.,
133 unit mass resolution, UMR) using SoFi (version 6.3) in Igor Pro (Paatero, 1999; Canonaco et
134 al., 2013). The data and error matrices were preprocessed according to Elser et al., (2016) and
135 detailed description of PMF analysis was given elsewhere (Canonaco et al. 2013; Elser et al
136 2016). Unconstrained PMF solutions with varied factor numbers were analyzed and six factors
137 were resolved, including two primary and four secondary organic factors (Fig. 3). The six-factor
138 solution was preferred because the five-factor solution was not able to separate high signal of
139 m/z 44 (which represents high oxidation state) from primary organic aerosol (POA) factors,
140 while the seven-factor solution added additional OOA factors with similar profiles and noisy
141 time series for which no physical interpretation could be found. The two POA factors consisted
142 of a traffic-related factor (hydrocarbon-like OA, HOA) and a cooking-related factor (COA),
143 which had been resolved in previous summer studies in NCP (Elser et al., 2016; Hu et al., 2016b;
144 Sun et al., 2016; Huang et al., 2019). AMS source apportionment studies often report one or
145 two oxygenated organic aerosol (OOA) factors that are distinguished by the extent of
146 oxygenation and linked to volatility or oxidation degree. Owing to higher mass resolution of
147 LTOF-AMS and the inclusion of integer-mass signals for m/z from 121 to 300 for high-
148 molecular-weight species such as polycyclic aromatic hydrocarbons (PAHs), we herein
149 resolved four SOA factors. These four SOA factors include aq-SOA attributable to aqueous-
150 phase chemistry, O_x-initiated-SOA attributable to photochemistry, primary-related-SOA
151 attributable to prompt oxidation of POA during emission, and fresh-SOA with a lower f_{44}/f_{43}
152 ratio (fraction of m/z 44 and 43 in OA).

153 **2.4 Aerosol liquid water content**

154 The aerosol liquid water content (ALWC) was simulated by ISORROPIA-II model (Fountoukis
155 and Nenes, 2007; Hennigan et al., 2015) using the measurements of ambient inorganic species
156 (NO₃, SO₄, NH₄, and Chl) and meteorological parameters (temperature and RH). The
157 simulation was run in “metastable” mode where all components are assumed to be deliquescent
158 and contain no solid matter. The concentrations and speciation (if dissociated) of those
159 inorganic species in thermodynamic equilibrium was then simulated by the model and then the
160 ALWC was calculated. The inorganic cations such as Na⁺, K⁺, Ca²⁺, Mg²⁺ were not measured
161 and included in the simulation on account of that these crustal ions constituted relatively small
162 fractions of aerosol, and had relatively weak effects on ALWC accumulation (Fountoukis and
163 Nenes, 2007; Su et al., 2022). The ISORROPIA-II model does not consider the contribution
164 to ALWC from organics, since inorganic aerosols dominate the water uptake by ambient
165 particles with a contribution of approximate >80% of the total ALWC (Huang et al., 2020).

166 **3. Results and discussion**

167 **3.1 SOA sources**

168 In our study, SOA accounted for 69% (13.5 $\mu\text{g m}^{-3}$) of the total OA (19.6 $\mu\text{g m}^{-3}$),
169 representing the dominant fraction in OA in summer Handan. Among the four PMF-resolved
170 SOA sources (Fig. 1), O_x-initiated-SOA dominated (31% to total OA), followed by fresh-SOA
171 (18%), aq-SOA (15%), and primary-related-SOA (5%). Since we focus on SOA formation in
172 this study, detailed descriptions of the HOA (12%) and COA (19%) is provided in section 1.1
173 in the SI. The mass spectral profiles of the six OA source factors are shown in Fig. 1, while the
174 time series of the SOA factors are shown in Fig. 2. In particular, a remarkable continuous
175 growth of aq-SOA concentration (from $\sim 0.3 \mu\text{g m}^{-3}$ to $25.2 \mu\text{g m}^{-3}$) and ALWC (from $3.1 \mu\text{g m}^{-3}$
176 to $486.1 \mu\text{g m}^{-3}$) occurred on 24th-28th August (Fig. 2d). Meanwhile, the O:C ratio indicative
177 of OA oxidation state displayed a continuous increase from 0.52 to a maximum of 0.93 during
178 this time (Fig. 2e), consistent with the continuous increase in RH (reaching over 95%). This
179 observation hints that during this period aqueous-phase processing might have played an
180 important role in aq-SOA formation. This role of aqueous-phase processing in SOA formation
181 is not just specific to this particular event, but also important in the whole campaign, which is
182 discussed in detail in section 3.3 later.

183 SOA factors were resolved depending on the oxidation state, which correspond to aged SOA
184 and fresh SOA respectively (Jimenez et al., 2009). One factor is attributed to aqueous-phase
185 chemistry (aq-SOA) and the other to photochemistry (O_x-initiated-SOA), while fresher factor
186 is produced by fresh-source (fresh-SOA) with a lower f_{44}/f_{43} ratio, and the other considered as

187 oxidized primary sources denoted as primary-related-SOA. Although all of the SOA factors
188 were characterized by higher m/z 44 (CO_2^+) and m/z 28 (CO^+) signal compared with POA
189 factors, their mass spectrum and temporal trends were noticeably distinguishable,
190 corresponding to different formation mechanism, which will be discussed in the following
191 section.

192 As shown in Fig. S3, the aq-SOA was identified as it increased with ALWC but decreased
193 with O_x , which might be produced/influenced by aqueous-phase chemistry and is defined as aq-
194 SOA. This indicates that aq-SOA was either formed via aqueous phase reactions or
195 absorbed/dissolved into aerosol liquid water. It exhibits the highest O:C ratios of all factors (0.7)
196 and a higher $f_{\text{CO}_2^+}$ to the total signal of 21.7%, but a low H:C ratio of 1.24 (Fig. 1). The O_x -
197 initiated-SOA in our study is photochemical production SOA whose formation initiated with
198 the presence of O_x . As O_x has been shown to be a conserved tracer to during photochemical
199 processing (Xu et al., 2017), the relationship between O_x and O_x -initiated-SOA can represent a
200 metric to characterize SOA formation mechanisms associated with ozone production chemistry
201 SOA (Herndon et al., 2008). O_x -initiated-SOA presented an opposite trend with significant
202 increase as function of O_x but decreased as a function of ALWC (Fig. S3), suggesting the
203 dominant role of photochemical processing in the formation of O_x -initiated-SOA.

204 The fresh-SOA showed an increase substantially as ALWC increasing, similar to aq-SOA.
205 Whereas it also showed a slight increase trend following O_x when $\text{O}_x < 100$ ppb (Fig. S3).
206 Therefore, both aqueous-phase chemistry and photochemical processing were thought to have
207 positive impacts synchronously on the formation of fresh-SOA. In this study, the fresh-SOA
208 had the lowest atomic O:C ratio of 0.41 and the highest atomic H:C ratio of 1.41 among the
209 four SOA factors, corresponding with the $f_{\text{CO}_2^+}$ of 8.3%, these characteristics are consistent with
210 the global average O:C ratio of LO-OOA of 0.35 ± 0.14 , Ng et al., 2010), demonstrating the it
211 is more fresh SOA. Although the primary-related-SOA constituted a small fraction and showed
212 little variation, this SOA source is also of particular interest because of its distinctive fragments
213 with high m/z values in the mass spectrum (Fig. 1d). At $m/z < 120$, the primary-related-SOA
214 had higher intensities for m/z 43 (mainly $\text{C}_2\text{H}_3\text{O}^+$) and m/z 44 (mainly CO_2^+) than those in POA,
215 indicating a typical nature of less-oxidized SOA. At $m/z > 120$, PAH-derived fragments are
216 clearly evident in the mass spectrum of the primary-related-SOA, as indicated by PAH-like ions
217 (described in SI 1.2) (Dzepina et al., 2007). Previous AMS studies have observed pronounced
218 peaks of PAH ions in POA mass spectra, such as those in coal combustion organic aerosol
219 (CCOA) and biomass burning organic aerosol (BBOA) (Hu et al., 2016b; Zhao et al., 2019),
220 but rarely in SOA. This observation implies that the factor may be related to the POA originated
221 from domestic coal combustion and here it is termed as primary-related-SOA (Xu et al., 2006).
222 Moreover, this SOA factor exhibited relatively better correlations with some gaseous pollutants
223 (Fig. S4), such as CO ($R = 0.6$) and NO_2 ($R = 0.5$), and also tracked with HOA ($R = 0.4$). These

224 observations suggest that the primary-related-SOA might be transformed from locally emitted
225 POA as a non-negligible source to SOA.

226 To further investigate the SOA formation mechanism, the dataset was segregated into three
227 periods according to different features depends on meteorological parameters (Fig. 2), i.e., the
228 reference period (P1), high-O_x period (P2) and high-RH period (P3). Briefly, the reference
229 period, P1, was characterized by a low average OA concentration ($15.4 \pm 3.2 \mu\text{g m}^{-3}$) and was
230 mainly affected by clean air from southwest of the sampling site and precipitation activities
231 (Table S1). The high-O_x period (P2) was featured by a high O_x concentration (65.1 ± 20.4 ppb),
232 warmer temperatures (26.4 ± 4.0 °C) but lower RH (57.7 ± 17.5 %). The mass loadings of OA
233 ($19.8 \pm 4.7 \mu\text{g m}^{-3}$) and other pollutants in P2 were higher than those in P1 (Table S1). P3 was
234 assigned as a high-RH period because of the noticeably high RH (83.7 ± 12.5 %) and high
235 ALWC ($95.4 \pm 114.2 \mu\text{g m}^{-3}$). Winds were weak ($<1.0 \text{ m s}^{-1}$) throughout this period, indicative
236 of stagnant conditions, which facilitated pollutant accumulation and resulted in the highest
237 average OA concentrations ($25.0 \pm 6.2 \mu\text{g m}^{-3}$).

238 During the reference period (P1), SOA had the lowest contribution to OA (57%), and the O_x-
239 initiated-SOA and aq-SOA constituted 22% and 21% to total OA, respectively. For the high-
240 O_x period (P2), enhanced SOA formation was found, with the SOA fraction increased to 71%
241 of the total OA. The O_x-initiated-SOA showed the highest mass loading of $7.3 \mu\text{g m}^{-3}$ and
242 highest contribution of 37% to total OA. These increases suggest that high-O_x condition
243 facilitates the production of SOA by photochemistry, making the O_x-initiated-SOA the major
244 source of SOA during P2. During the high-RH period (P3), SOA fraction continually increased,
245 approaching 79% in total OA, and the SOA was mainly contributed by aq-SOA and fresh-SOA.
246 The mass contribution of aq-SOA increased dramatically from 9% to total OA during P2 to 33%
247 during P3 (Fig. S2), and average mass concentrations from $1.8 \mu\text{g m}^{-3}$ to $8.3 \mu\text{g m}^{-3}$, which
248 suggests rapid SOA production through the aqueous-phase chemistry. Comparatively, the
249 contribution of fresh-SOA was about ~20% in both P2 and P3, but lower in P1 (9%), suggesting
250 that the formation fresh-SOA was affected by both high O_x and high RH. It should also be noted
251 that O:C ratio increased in the succession from P1 (0.73) to P2 (0.74) and further to P3 (0.77),
252 accompanied by continually decrease of H:C ratio from 1.64 to 1.56, and to 1.53 (Fig. 3),
253 suggesting the increase of OA oxidation degree. As a result, the high O_x in P2 and high RH in
254 P3 (as compared to P1) promoted the formation of SOA, specifically O_x-initiated-SOA (in P2)
255 and aq-SOA (in P3), leading to the increase in the degree of oxygenation in total OA.

256 Overall, our results suggest that SOA could be formed through different pathways, in
257 particular photochemistry, aqueous-phase chemistry, and conversion of POA to SOA
258 contributed to SOA formation.

259 3.2 Photochemistry

260 As expected for summertime, photochemistry associated with O_x has significant impacts on
261 the formation and evolution of SOA. Herein, the relationships between OA factors and O_x were
262 investigated to offer insights into the formation mechanisms of SOA associated with the ozone
263 production chemistry (Herndon et al., 2008). During P2, as O_x increased, the mass loadings of
264 O_x -initiated-SOA showed a substantially increasing trend when O_x was > 30 ppb and eventually
265 saturated when O_x was >100 ppb, raising the contribution of O_x -initiated-SOA from 20% to 61%
266 of total OA (Fig. 4). This observation indicates the importance of photochemistry in the
267 formation of O_x -initiated-SOA in summer, in which high O_x concentration as well as
268 temperature corresponding to strong atmospheric oxidative capacity, can accelerate the
269 photochemical formation (Duan et al., 2021). As a comparison, the mass concentrations of other
270 OA factors except O_x -initiated-SOA showed decreasing trends as O_x increased (Fig. 4c). Such
271 differences between SOA factors are likely due to the enhanced secondary
272 production/transformation from POA and fresher SOA factors to the more aged O_x -initiated-
273 SOA. Note that the O:C ratio presented a faster increasing rate as a function of O_x (from 0.6 to
274 1.0, Fig. 4d) than those in P1 and P3, suggesting that photochemistry might result in higher OA
275 oxidation state during P2.

276 The typical episode with high- O_x period (P2) was dominated by a series of daytime
277 photochemical evolutions. To evaluate the relative contributions of photochemical and
278 aqueous-phase processing production and the transformation of these SOA factors in different
279 meteorological stages, the average diurnal variations of OA factors, O:C ratios, O_x , temperature,
280 AWLC and primary gas pollutants during different periods are shown for comparison. Fig. 6
281 shows that O_x increased rapidly from 6:00 to 14:00 in all periods, but was highest in
282 P2. Correspondingly, a lower mean value of ALWC ($8.4 \mu\text{g m}^{-3}$) was also observed in P2 than
283 in P1 and P3. During P2, O_x -initiated-SOA was produced quickly and played the dominant role
284 during daytime, while its concentration typically decreased during nighttime. The average
285 concentration of O_x -initiated-SOA increased continually from $4.2 \mu\text{g m}^{-3}$ at 7:00 local time (LT)
286 to $10.4 \mu\text{g m}^{-3}$ at 15:00 LT in 8 h, with the maximum O_x -initiated-SOA mass fraction in OA
287 reaching 65% at 15:00 LT (Fig. S6c). This high average growth rate of $0.8 \mu\text{g m}^{-3} \text{h}^{-1}$ in O_x -
288 initiated-SOA corresponded to the high O_x concentration, high temperature and strong solar
289 radiation in daytime, suggesting enhanced photochemistry reaction. In contrast, the
290 concentrations and the contributions of other SOA factors decreased continuously at the same
291 time (Fig. 6). The opposite trends between O_x -initiated-SOA and other OA factors from 7:00
292 to 15:00 LT suggest that some part of POA and fresh-SOA may convert to O_x -initiated-SOA
293 by photochemical oxidation. This conclusion is consistent with findings reported by Li et al.,
294 (2020) in urban Beijing, where less-oxidized SOA may transform to more-oxidized SOA
295 through photochemical processing as well. The O:C ratio of OA presented a significant
296 increasingly diurnal variation with a noon peak around 14:00 ~ 16:00 LT in P2, which had the

297 highest value of 0.74 compared with P1 and P3, suggesting the potential transformation from
298 POA factors and fresh SOA factors to O_x -initiated-SOA could also noticeably affect OA
299 characteristics such as oxidation state in summer daytime. It is further indicated by a small
300 afternoon peak of the more oxidized tracer CO_2^+ (m/z 44) and the decrease in a less oxidized
301 tracer $C_2H_3O^+$ (m/z 43) (Fig. 7b). As a result, the mass spectra, which were initially fresh SOA
302 products evolved to become aged SOA products as the photochemical age increased. Overall,
303 with little water in the particles, the high solar radiation and high O_x concentration during
304 daytime associated with a relatively high degree of oxygenation of OA suggest that gas-phase
305 oxidation and partitioning processes are probably the dominating process in SOA formation
306 during P2.

307 In addition, these results further support the idea that during the high- O_x period of summer,
308 photochemistry has significant impacts on SOA formation, especially on O_x -initiated-SOA.
309 Note that the role of photochemistry in the formation of O_x -initiated-SOA is not only limited to
310 the gas-phase photochemistry, but also can also occur in the aqueous phase (Kuang et al., 2020).
311 This is the case for P3 in our study, which is discussed further in section 3.3 below.

312 **3.3 Aqueous-phase chemistry**

313 The aqueous-phase chemistry has imposed significant impacts on SOA formation during this
314 field campaign. To further explore the formation mechanism of SOA associated with aqueous-
315 phase chemistry, the relationships between different OA factors and ALWC were investigated.
316 During P3, the mass concentration of aq-SOA increased from $5 \mu g m^{-3}$ to $17 \mu g m^{-3}$, yet its
317 fraction showed a particularly pronounced rise from 22.5% to 52% of total OA when ALWC
318 increased from 0.3 to $200 \mu g m^{-3}$ (Fig. 5e and f). Note that there are still consistent mass
319 concentrations of aq-SOA even when ALWC is very low (data interval ranging from 0~40 μg
320 m^{-3}), which is due to that over 80% of ALWC mass concentration were loaded in the first
321 interval, leading to a higher mean value of aq-SOA mass concentration. Actually ALWC
322 showed quite low mass loading in most period time but increased dramatically during P3, yet
323 the time series of aq-SOA and ALWC were remarkably well correlated throughout the entire
324 campaign ($R=0.7$, Fig. S4) rather than a strong correlation observed only in P3. This general
325 correlation further confirms the important role of aqueous-phase chemistry in the formation of
326 aq-SOA and characterized the aqueous-phase formation of aq-SOA throughout the campaign
327 rather than only in the high-RH event as shown in section 3.1 earlier. We also found that the
328 concentration and fraction of aq-SOA became stable when ALWC was $> 200 \mu g m^{-3}$, which is
329 probably attributable to that the aq-SOA formation within droplets was soon outweighed by the
330 scavenging processes when RH was high enough ($> 95\%$). The O:C ratio shows an obvious
331 increase from 0.7 to around 0.85 when ALWC increases to $200 \mu g m^{-3}$, after which it remains

332 relatively stable (0.85) as the ALWC increases further (Fig. 5). These results suggest that
333 aqueous-phase chemistry can affect the oxidation degree of OA by changing SOA composition,
334 especially the enhanced contribution of aq-SOA. However, the growth rate of O:C ratios as
335 ALWC increases in P3 was lower than that in P2 (up to 1 as O_x increases). Also, the correlation
336 between O:C vs. O_x in P2 ($R=0.6$) was stronger than O:C vs. ALWC ($R=0.3$) (Fig. S8).

337 Fig. 6 illustrate the different types of aqueous-phase chemistry in daytime and nighttime.
338 During the nighttime in P3, aqueous-phase oxidation was also enhanced during nighttime
339 (19:00–07:00 LT). As shown in Fig. 6, O:C ratio (0.76) at nighttime in P3 was higher than those
340 in P2, while exhibiting a much smaller peak during daytime. Compared with the low ALWC in
341 P2, the much higher ALWC concentration (peak value of $235.9 \mu\text{g m}^{-3}$ at 2:00 LT) and higher
342 RH (peak value of 93.7% at 6:00 LT) during nighttime in P3 suggested a dominant contribution
343 by aqueous-phase processing. The aq-SOA shows a quite clear and unique diurnal pattern in
344 P3, with much higher mass concentration during the whole day (especially at nighttime) than
345 those in P1 and P2. After 17:00 LT, aq-SOA started to increase from $4.7 \mu\text{g m}^{-3}$ to $12.7 \mu\text{g m}^{-3}$
346 at 7:00 LT, which showed a rapid nighttime growth rate of $0.6 \mu\text{g m}^{-3} \text{h}^{-1}$, indicating enhanced
347 SOA formation through aqueous-phase chemistry at night. Whereas O_x -initiated-SOA
348 decreased rapidly from $8.2 \mu\text{g m}^{-3}$ at 17:00 LT until reaching its lowest concentration of 2.6
349 $\mu\text{g m}^{-3}$ until the morning, suggesting the gas-to-particle partitioning at night under high ALWC
350 conditions. Furthermore, this transformation could be supported by the increase in CO_2^+ (m/z
351 44) and the decrease in a less oxidized tracer $\text{C}_2\text{H}_3\text{O}^+$ (m/z 43) at night (Fig. 7c). Since when
352 the ALWC is sufficiently high, it was likely to accommodate much of the precursor organics
353 and oxidants to low-volatility products through aqueous-phase oxidation. In addition, the dark
354 aqueous-phase SOA formation was likely strong enough to counteract the nighttime scavenging
355 processes under high-RH conditions. Therefore, the dark aqueous-phase chemistry forming aq-
356 SOA shows a dominant role (over 40% to OA) during nighttime in P3.

357 However, during the daytime, the mass concentration of aq-SOA decreased from 7:00 to
358 17:00 LT in P3, coinciding an obvious increase trend of O_x -initiated-SOA at the same time with
359 an average growth rate of $0.6 \mu\text{g m}^{-3} \text{h}^{-1}$ (Fig. 6). This phenomenon suggests photochemical
360 processing can also occur in the aqueous phase when RH and ALWC were still high.
361 Photochemical reactions through both aqueous-phase and gas-phase can contribute
362 substantially to the SOA formation in polluted areas of NCP, and during haze days with high
363 RH and ALWC the aqueous-phase photochemical processes played a dominant role in daytime
364 SOA formation (Kuang et al., 2020). The rapid daytime O_x -initiated-SOA formation in our
365 study possibly occurred on the particle surface and in the aerosol liquid water (Ervens et al.,
366 2011) under humid conditions with high ALWC but driven by gas-phase direct photolysis and
367 oxidation by photooxidants under high O_x conditions. Under such high-RH level ($\text{RH} > 80\%$),

368 the water-soluble species produced from photochemistry in the gas phase can also partition into
369 the aqueous phase and be further oxidized to form low-volatility products (Carlton et al., 2007;
370 Sullivan et al., 2016). Previous studies have demonstrated that gas-phase oxidants such as OH
371 radicals and H₂O₂ can also partition to the aqueous phase to further oxidize dissolved the
372 oxidized VOCs (OVOCs) into aq-SOA (Ye et al., 2018). Other studies also revealed that
373 photochemical reactions in the aqueous droplets can occur through direct photolysis or through
374 oxidation by oxidants (Ervens et al., 2011; 2014; Ye et al., 2018). Therefore, in our campaign,
375 dark aqueous-phase chemistry is responsible for rapid aq-SOA formation during nighttime,
376 while the aqueous-phase photochemistry during daytime is likely prevail by rapid daytime O_x-
377 initiated-SOA formation during P3. This comparison demonstrates that the nocturnal aqueous-
378 phase chemistry and daytime aqueous-phase photochemistry are both important pathways in
379 the total SOA growth. The aqueous-phase chemistry related to fresh-SOA is more complicated,
380 requiring both daytime radiative conditions and certain amounts of ALWC in nighttime. For
381 example, Fig. 5e shows that the fresh-SOA has a similar increasing trend with aq-SOA as
382 ALWC increased, however, it also increased slightly as O_x increased (Fig. 4e), hinting that both
383 ALWC and the oxidants are critical for fresh-SOA formation and both the aqueous-phase
384 chemistry and the photochemistry (including that in the aqueous phase) participated to produce
385 fresh-SOA simultaneously. It is worth noting that three peaks were found in the diurnal
386 variation of fresh-SOA in P3. The peaks at around 6:00 and 19:00 LT at night were similar to
387 those of aq-SOA and lower than it, while the peak at around 13:00 LT is consistent with the
388 peak in the diurnal cycle of O_x (Fig. 6). Although there is also a smaller peak around 13:00 LT
389 in P3, the whole pattern of aq-SOA is characterized by decreasing trend at daytime. These
390 results suggest that fresh-SOA could be formed through dark nighttime aqueous-phase reactions,
391 which are partially reversible upon the evaporation of aerosol liquid water, and also formed
392 through photochemical aqueous-phase reactions during daytime. Different from aq-SOA,
393 which is highly correlated and limited with ALWC, two types of aqueous-phase chemistry in
394 daytime and nighttime are dominant pathways to the fresh-SOA growth. Our analysis on
395 formation pathways of these SOA factors suggested the potential interactive roles of gas-phase
396 oxidation, gas-particle partitioning, and aqueous-phase oxidation in the formation of SOA.

397 **3.4 SOA from POA transformation**

398 The photochemistry and aqueous-phase chemistry show distinct effects on POA evolution
399 and SOA formation. The relationships between O_x-initiated-SOA /aq-SOA and other POA-
400 related components (HOA + COA + primary-related-SOA) were plotted in Fig. S9. A strong
401 negative correlation ($R=-0.8$) between POA-related components and O_x-initiated-SOA was
402 observed (Fig. S9c), consistent with the decrease in mass concentration of POA-related
403 components during P2. This observation suggests that the production of O_x-initiated-SOA was

404 at least partly facilitated by photochemical transformation of other OA components. However,
405 the better diffusion conditions in P2 might also attribute a great extent to the negative
406 correlation, as the formation period of O_x -initiated-SOA usually occurred during the noontime
407 when the boundary layer was much developed, while the POA usually decreased via horizontal
408 and vertical diffusion. In comparison, POA-related components and aq-SOA correlate weakly.
409 When ALWC ($<20 \mu\text{g m}^{-3}$) and nitrate concentrations were lower ($< 3 \mu\text{g m}^{-3}$), mostly during
410 P1 and P2, POA-related components and aq-SOA showed almost no correlation ($R=0.1$ and $R=-$
411 0.1). However, when ALWC concentration and nitrate concentration were higher than those
412 thresholds above (data points with yellow/red colors mostly during P3), they had a relatively
413 good negative correlation ($R=-0.5$) (Fig. S9f), indicating the importance of ALWC and nitrate
414 in aqueous-phase chemistry. This is consistent with results in winter Beijing (Wang et al., 2021),
415 where POA factor had strong negative correlations with aq-SOA, suggesting that these POA
416 factors might produce aq-SOA by aqueous-phase oxidation. In addition, under high-ALWC
417 conditions, nitrate had similar formation mechanisms with aq-SOA or high nitrate supports the
418 potential formation/transformation from POA-related components to aq-SOA, which is
419 consistent with the results in section 3.3. The phenomenon of negative correlation between
420 POA-related components and SOA at high O_x /ALWC further emphasizes the importance of
421 conversion from POA to SOA.

422 As shown in the Van Krevelen (VK) plot (Fig. 8a), O:C and H:C both increase in the
423 succession from primary-related-SOA to O_x -initiated-SOA and eventually to aq-SOA,
424 supporting a successive oxidation sequence from primary-related-SOA to aq-SOA. Generally,
425 H:C shows a decreasing trend as O:C increases for organic compounds during oxidation in
426 other studies (Ng et al., 2011; Gilardoni et al., 2016; Lee et al., 2017; Zhao et al., 2019; Chen
427 et al., 2021), suggesting a general negative correlation between H:C and O:C. This positive
428 relationship of O:C and H:C evolution during oxidative aging in this study is interesting. It
429 might be caused by ring-breaking reactions which could further promote the transformation of
430 aromatic POA to aq-SOA. Previous studies in both laboratory (Huang et al., 2018; Wang et al.,
431 2020) and field (Hu et al., 2016a) demonstrated that the OH-initiated ring-breaking reactions
432 of aromatic species can occur in the aqueous phase and form highly oxidized oxygenated
433 compounds. For example, Hems and Abbatt (2018) suggested that nitrophenol molecules could
434 react rapidly with OH radicals in aqueous solutions with the addition of OH functional groups
435 to the aromatic ring at the initial stage, followed by fragmentation to multifunctional organic
436 species with high H:C and O:C ratios. Wang et al. (2021) found that the ring-breaking oxidation
437 of aromatic FF-POA was the mechanism for aq-SOA formation. Similar to those in primary-
438 related-SOA, PAH-like ions was also found in the mass spectrum of aq-SOA at $m/z > 150$,
439 albeit less pronounced, consistent with a previous study in Beijing (Wang et al., 2021). This is
440 likely due to the oxidation of PAHs in the conversion of primary-related-SOA and aq-SOA,

441 which is caused by enhanced hydroxylation of the aromatic ring and increased yields of
442 carboxylic acids in OH-initiated reactions (Sun et al., 2010). This kind of ring-breaking
443 oxidation of aromatic POA could thus lead to aq-SOA formation (Huang et al., 2018; Wang et
444 al., 2021). In addition, the locations of aq-SOA and the slope of overall OA are near the line
445 with the slope of -1 in the VK plot, indicating more carboxylic acid formation while the
446 replacement of a hydrogen atom with a carboxylic acid group ($-\text{COOH}$) (Heald et al., 2010;
447 Ng et al., 2011). This observation supports that oxidation of PAHs was probably involved in
448 the conversion of primary-related-SOA to aq-SOA through aqueous-phase chemistry, leading
449 to functionalization as carbonyls and carboxylic acids.

450 Specifically, the organic fragments and mass spectrum evolution of OA were analyzed to
451 illuminate the transformation in photochemical processing and aqueous-phase chemistry. Fig.
452 8b shows the mass fractions of CH_2O_2^+ , CH_3SO^+ , HCO_2^+ , and $\text{C}_2\text{H}_2\text{O}_2^+$ ion fragments in OA as
453 a function of ALWC. The aq-SOA was tightly correlated with CH_2O_2^+ ($R^2 = 0.81$) at m/z 46
454 and CH_3SO ($R^2 = 0.78$) at m/z 63 (Fig. S10). Consistently, both of them showed increase trends
455 as ALWC increasing, similar as aq-SOA, which indicating typical fragment characteristics of
456 ions of aqueous-phase processing products (Tan et al., 2009; Sun et al., 2016; Duan et al., 2021).
457 The intensities of HCO_2^+ (m/z 45), a common fragment ion of carboxylic acids, is associated
458 with aqueous oxidation of aromatic compounds. $\text{C}_2\text{H}_2\text{O}_2^+$ (m/z 58) is a tracer ion for glyoxal,
459 which could be a ring-breaking product from the aqueous-phase oxidation of PAHs. The
460 increasing trends of these ions with ALWC suggest that water-soluble organic species such as
461 carboxylic acids and glyoxal are produced as components of aq-SOA following aromatic
462 oxidation and ring breaking. Moreover, the concentration of PAHs increased with the increase
463 of ALWC (Fig. S11), consistent with the oxidation of PAHs from ring-breaking reactions that
464 can take place in the aqueous phase and being involved in the conversion to aq-SOA.

465 **4. Conclusion**

466 The sources and formation mechanisms of SOA were investigated by online aerosol mass
467 spectrometry and statistical (PMF) analysis from August to September of 2019 in Handan, a
468 mid-sized industrialized city in NCP of China. Four specific SOA factors were resolved,
469 including aq-SOA (15% to total OA), O_x -initiated-SOA (31%), fresh-SOA (18%) and primary-
470 related-SOA (5%). By studying the formation of these SOA factors in different selected periods
471 (P1-P3) against O_x and ALWC, we found multiple pathways leading to their formation,
472 sometimes with mixed pathways for one type of SOA.

473 Both photochemistry and aqueous-phase chemistry resulted in enhanced OA oxidation state.
474 During high- O_x period, photochemistry had imposed significant impacts on the formation and
475 evolution of SOA in summertime. The O_x -initiated-SOA contributed up to 65% to total OA in

476 the daytime, with a high average growth rate of $0.8 \mu\text{g m}^{-3} \text{h}^{-1}$, suggesting the efficient daytime
477 formation of SOA from photochemistry. Rapid increases of the concentration and contribution
478 (up to 61%) of O_x -initiated-SOA were found as O_x increased, while all the other OA factors
479 showed decreasing trends with O_x concentration increasing. The difference suggests enhanced
480 secondary transformation from POA/fresh SOA factors to the more aged O_x -initiated-SOA
481 under high- O_x condition. However, during the high-RH period, two types of aqueous-phase
482 chemistry were both important pathways for the SOA growth. During nighttime and under high-
483 RH conditions, dark aqueous-phase chemistry played significant roles with rapid aq-SOA
484 formation (up to 45% in total OA), while the aqueous-phase photochemistry was more
485 important by rapid O_x -initiated-SOA formation during daytime (up to 39% in total OA). The
486 primary-related-SOA was evidently linked to the POA originated from coal combustion
487 activities, as indicated by the PAH-like ion peaks. Although it constituted a small fraction of
488 5%, the potential transformation and conversion from primary-related-SOA to aq-SOA could
489 also be an important pathway via hydroxylation of the aromatic ring or ring-breaking oxidation
490 of aromatic POA species through aqueous-phase chemistry. This study highlights the multiple
491 reaction pathways, on top of multiple precursor types, on the SOA formation in industrialized
492 regions, and calls form more in-depth study on the interactive roles of those formation pathways.

493

494 **Data availability.** Raw data used in this study are archived at the Institute of Earth Environment,
495 Chinese Academy of Sciences, and are available on request by contacting the corresponding
496 author.

497 **Supplement.** The Supplement related to this article is available online.

498 **Competing interests.** The authors declare that they have no conflict of interest.

499 **Author contributions.** RJH designed the study. Data analysis and source apportionment were
500 done by YFG and RJH. YFG and RJH wrote the manuscript. YFG and RJH interpreted data
501 and prepared display items. All authors commented on and discussed the manuscript.

502 **Acknowledgement**

503 This work was supported by the National Natural Science Foundation of China (no.
504 41925015), the Key Research Program of Frontier Sciences from the Chinese Academy of
505 Sciences (no. ZDBS-LY-DQC001), the Strategic Priority Research Program of the Chinese
506 Academy of Sciences (no. XDB40000000), and SKLLQG (no. SKLLQGTD1801).

507

508 **References**

- 509 An, Z., Huang, R. J., Zhang, R., Tie, X., Li, G., Cao, J., Zhou, W., Shi, Z., Han, Y., Gu, Z., and
510 Ji, Y.: Severe haze in northern China: A synergy of anthropogenic emissions and
511 atmospheric processes, *Proc. Natl. Acad. Sci. U. S. A.*, 116, 8657–8666,
512 <https://doi.org/10.1073/pnas.1900125116>, 2019.
- 513 Bikkina, S., Kawamura, K., and Sarin, M.: Secondary Organic Aerosol Formation over Coastal
514 Ocean: Inferences from Atmospheric Water-Soluble Low Molecular Weight Organic
515 Compounds, *Environ. Sci. Technol.*, 51, 4347–4357,
516 <https://doi.org/10.1021/acs.est.6b05986>, 2017.
- 517 Canagaratna, M. R., Jimenez, J. L., Kroll, J. H., Chen, Q., Kessler, S. H., Massoli, P.,
518 Hildebrandt Ruiz, L., Fortner, E., Williams, L. R., Wilson, K. R., Surratt, J. D., Donahue, N.
519 M., Jayne, J. T., and Worsnop, D. R.: Elemental ratio measurements of organic compounds
520 using aerosol mass spectrometry: Characterization, improved calibration, and implications,
521 *Atmos. Chem. Phys.*, 15, 253–272, <https://doi.org/10.5194/acp-15-253-2015>, 2015.
- 522 Canonaco, F., Crippa, M., Slowik, J. G., Baltensperger, U., and Prévôt, A. S. H.: SoFi, an
523 IGOR-based interface for the efficient use of the generalized multilinear engine (ME-2) for
524 the source apportionment: ME-2 application to aerosol mass spectrometer data, *Atmos.*
525 *Meas. Tech.*, 6, 3649–3661, <https://doi.org/10.5194/amt-6-3649-2013>, 2013.
- 526 Carlton, A. G., Turpin, B. J., Altieri, K. E., Seitzinger, S., Reff, A., Lim, H. J., and Ervens, B.:
527 Atmospheric oxalic acid and SOA production from glyoxal: Results of aqueous
528 photooxidation experiments, *Atmos. Environ.*, 41, 7588–7602,
529 <https://doi.org/10.1016/j.atmosenv.2007.05.035>, 2007.
- 530 Chen, W., Ye, Y., Hu, W., Zhou, H., Pan, T., Wang, Y., Song, W., Song, Q., Ye, C., Wang, C.,
531 Wang, B., Huang, S., Yuan, B., Zhu, M., Lian, X., Zhang, G., Bi, X., Jiang, F., Liu, J.,
532 Canonaco, F., Prevot, A. S. H., Shao, M., and Wang, X.: Real-time characterization of
533 aerosol compositions, sources and aging processes in Guangzhou during PRIDE-GBA 2018
534 campaign, *J. Geophys. Res. Atmos.*, <https://doi.org/10.1029/2021jd035114>, 2021.
- 535 Cohen, A. J., Brauer, M., Burnett, R., Anderson, H. R., Frostad, J., Estep, K., Balakrishnan, K.,
536 Brunekreef, B., Dandona, L., Dandona, R., Feigin, V., Freedman, G., Hubbell, B., Jobling,
537 A., Kan, H., Knibbs, L., Liu, Y., Martin, R., Morawska, L., Pope, C. A., Shin, H., Straif, K.,
538 Shaddick, G., Thomas, M., van Dingenen, R., van Donkelaar, A., Vos, T., Murray, C. J. L.,
539 and Forouzanfar, M. H.: Estimates and 25-year trends of the global burden of disease
540 attributable to ambient air pollution: an analysis of data from the Global Burden of Diseases
541 Study 2015, *Lancet*, 389, [https://doi.org/10.1016/S0140-6736\(17\)30505-6](https://doi.org/10.1016/S0140-6736(17)30505-6), 2017.
- 542 Donahue, N. M., Robinson, A. L., Stanier, C. O., and Pandis, S. N.: Coupled partitioning,
543 dilution, and chemical aging of semivolatile organics, *Environ. Sci. Technol.*, 40,
544 <https://doi.org/10.1021/es052297c>, 2006.

- 545 Duan, J., Huang, R. J., Gu, Y., Lin, C., Zhong, H., Wang, Y., Yuan, W., Ni, H., Yang, L., Chen,
546 Y., Worsnop, D. R., and O'Dowd, C.: The formation and evolution of secondary organic
547 aerosol during summer in Xi'an: Aqueous phase processing in fog-rain days, *Sci. Total*
548 *Environ.*, 756, 144077, <https://doi.org/10.1016/j.scitotenv.2020.144077>, 2021.
- 549 Dzepina, K., Arey, J., Marr, L. C., Worsnop, D. R., Salcedo, D., Zhang, Q., Onasch, T. B.,
550 Molina, L. T., Molina, M. J., and Jimenez, J. L.: Detection of particle-phase polycyclic
551 aromatic hydrocarbons in Mexico City using an aerosol mass spectrometer, *Int. J. Mass*
552 *Spectrom.*, 263, 152–170, <https://doi.org/10.1016/j.ijms.2007.01.010>, 2007.
- 553 Elser, M., Huang, R., Wolf, R., Slowik, J. G., Wang, Q., Canonaco, F., Li, G., Bozzetti, C.,
554 Daellenbach, K. R., Huang, Y., Zhang, R., Li, Z., Cao, J., Baltensperger, U., El-haddad, I.,
555 and Prévôt, A. S. H.: New insights into PM_{2.5} chemical composition and sources in two
556 major cities in China during extreme haze events using aerosol mass spectrometry, 3207–
557 3225, <https://doi.org/10.5194/acp-16-3207-2016>, 2016.
- 558 Ervens, B., Turpin, B. J., and Weber, R. J.: Secondary organic aerosol formation in cloud
559 droplets and aqueous particles (aqSOA): A review of laboratory, field and model studies,
560 *Atmos. Chem. Phys.*, 11, 11069–11102, <https://doi.org/10.5194/acp-11-11069-2011>, 2011.
- 561 Ervens, B., Armin, S., B., L. Y., and J., and T. B.: Key parameters controlling OH-initiated
562 formation of secondary organic aerosol in the aqueous phase (aqSOA), *J. Geophys. Res.*,
563 6578–6595, <https://doi.org/10.1002/2013JD021021>.Received, 2014.
- 564 Fountoukis, C. and Nenes, A.: ISORROPIAII: A computationally efficient thermodynamic
565 equilibrium model for K⁺-Ca²⁺-Mg²⁺-NH₄⁺-Na⁺-SO₄²⁻-NO₃⁻-Cl⁻-H₂O aerosols, *Atmos.*
566 *Chem. Phys.*, 7, 4639–4659, <https://doi.org/10.5194/acp-7-4639-2007>, 2007.
- 567 Gilardoni, S., Massoli, P., Paglione, M., Giulianelli, L., Carbone, C., Rinaldi, M., Decesari, S.,
568 Sandrini, S., Costabile, F., and Gobbi, G. P.: Direct observation of aqueous secondary
569 organic aerosol from biomass-burning emissions, *Proc. Natl. Acad. Sci. U. S. A.*, 113,
570 10013–10018, <https://doi.org/10.1073/pnas.1602212113>, 2016.
- 571 Gu, Y., Huang, R. J., Li, Y., Duan, J., Chen, Q., Hu, W., Zheng, Y., Lin, C., Ni, H., Dai, W.,
572 Cao, J., Liu, Q., Chen, Y., Chen, C., Ovadnevaite, J., Ceburnis, D., and O'Dowd, C.:
573 Chemical nature and sources of fine particles in urban Beijing: Seasonality and formation
574 mechanisms, *Environ. Int.*, 140, 105732, <https://doi.org/10.1016/j.envint.2020.105732>,
575 2020.
- 576 Heald, C. L., Kroll, J. H., Jimenez, J. L., Docherty, K. S., Decarlo, P. F., Aiken, A. C., Chen,
577 Q., Martin, S. T., Farmer, D. K., and Artaxo, P.: A simplified description of the evolution
578 of organic aerosol composition in the atmosphere, *Geophys. Res. Lett.*, 37,
579 <https://doi.org/10.1029/2010GL042737>, 2010.
- 580 Hems, R. F. and Abbatt, J. P. D.: Aqueous Phase Photo-oxidation of Brown Carbon
581 Nitrophenols: Reaction Kinetics, Mechanism, and Evolution of Light Absorption, *ACS*
582 *Earth Sp. Chem.*, 2, 225–234, <https://doi.org/10.1021/acsearthspacechem.7b00123>, 2018.

- 583 Hennigan, C. J., Izumi, J., Sullivan, A. P., Weber, R. J., and Nenes, A.: A critical evaluation of
584 proxy methods used to estimate the acidity of atmospheric particles, *Atmos. Chem. Phys.*,
585 15, 2775–2790, <https://doi.org/10.5194/acp-15-2775-2015>, 2015.
- 586 Herndon, S. C., Onasch, T. B., Wood, E. C., Kroll, J. H., Canagaratna, M. R., Jayne, J. T.,
587 Zavala, M. A., Knighton, W. B., Mazzoleni, C., Dubey, M. K., Ulbrich, I. M., Jimenez, J.
588 L., Seila, R., de Gouw, J. A., de Foy, B., Fast, J., Molina, L. T., Kolb, C. E., and Worsnop,
589 D. R.: Correlation of secondary organic aerosol with odd oxygen in Mexico City, *Geophys.*
590 *Res. Lett.*, 35, <https://doi.org/10.1029/2008GL034058>, 2008.
- 591 Hu, W., Hu, M., Hu, W. W., Niu, H., Zheng, J., Wu, Y., Chen, W., Chen, C., Li, L., Shao, M.,
592 Xie, S., and Zhang, Y.: Characterization of submicron aerosols influenced by biomass
593 burning at a site in the Sichuan Basin, southwestern China, *Atmos. Chem. Phys.*, 16, 13213–
594 13230, <https://doi.org/10.5194/acp-16-13213-2016>, 2016a.
- 595 Hu, W., Hu, M., Hu, W., Jimenez, J. L., Yuan, B., Chen, W., Wang, M., Wu, Y., Chen, C.,
596 Wang, Z., Peng, J., Zeng, L., and Shao, M.: *Journal of Geophysical Research : Atmospheres*,
597 1955–1977, <https://doi.org/10.1002/2015JD024020>.Received, 2016b.
- 598 Hu, W., Palm, B. B., Day, D. A., Campuzano-Jost, P., Krechmer, J. E., Peng, Z., De Sa Suzane,
599 S., Martin, S. T., Alexander, M. L., Baumann, K., Hacker, L., Kiendler-Scharr, A., Koss, A.
600 R., De Gouw, J. A., Goldstein, A. H., Seco, R., Sjostedt, S. J., Park, J. H., Guenther, A. B.,
601 Kim, S., Canonaco, F., Prévôt, A. S. H., Brune, W. H., and Jimenez, J. L.: Volatility and
602 lifetime against OH heterogeneous reaction of ambient isoprene-epoxydiols-derived
603 secondary organic aerosol (IEPOX-SOA), *Atmos. Chem. Phys.*, 16, 11563–11580,
604 <https://doi.org/10.5194/acp-16-11563-2016>, 2016c.
- 605 Hu, W., Hu, M., Hu, W., Zheng, J., Chen, C., Wu, Y., and Guo, S.: Seasonal variations in high
606 time-resolved chemical compositions, sources, and evolution of atmospheric submicron
607 aerosols in the megacity Beijing, 9979–10000, 2017.
- 608 Huang, D. D., Zhang, Q., Cheung, H. H. Y., Yu, L., Zhou, S., Anastasio, C., Smith, J. D., and
609 Chan, C. K.: Formation and Evolution of aqSOA from Aqueous-Phase Reactions of
610 Phenolic Carbonyls: Comparison between Ammonium Sulfate and Ammonium Nitrate
611 Solutions, *Environ. Sci. Technol.*, 52, 9215–9224, <https://doi.org/10.1021/acs.est.8b03441>,
612 2018.
- 613 Huang, R. J., Zhang, Y., Bozzetti, C., Ho, K. F., Cao, J. J., Han, Y., Daellenbach, K. R., Slowik,
614 J. G., Platt, S. M., Canonaco, F., Zotter, P., Wolf, R., Pieber, S. M., Bruns, E. A., Crippa,
615 M., Ciarelli, G., Piazzalunga, A., Schwikowski, M., Abbaszade, G., Schnelle-Kreis, J.,
616 Zimmermann, R., An, Z., Szidat, S., Baltensperger, U., El Haddad, I., and Prévôt, A. S. H.:
617 High secondary aerosol contribution to particulate pollution during haze events in China,
618 *Nature*, 514, 218–222, <https://doi.org/10.1038/nature13774>, 2014.
- 619 Huang, R. J., Wang, Y., Cao, J., Lin, C., Duan, J., Chen, Q., Li, Y., Gu, Y., Yan, J., Xu, W.,
620 Fröhlich, R., Canonaco, F., Bozzetti, C., Ovadnevaite, J., Ceburnis, D., Canagaratna, M. R.,
621 Jayne, J., Worsnop, D. R., El-Haddad, I., Prevot, A. S. H., and O’Dowd, C. D.: Primary

- 622 emissions versus secondary formation of fine particulate matter in the most polluted city
623 (Shijiazhuang) in North China, *Atmos. Chem. Phys.*, 19, 2283–2298,
624 <https://doi.org/10.5194/acp-19-2283-2019>, 2019.
- 625 Huang, R. J., He, Y., Duan, J., Li, Y., Chen, Q., Zheng, Y., Chen, Y., Hu, W., Lin, C., Ni, H.,
626 Dai, W., Cao, J., Wu, Y., Zhang, R., Xu, W., Ovadnevaite, J., Ceburnis, D., Hoffmann, T.,
627 and D. O'Dowd, C.: Contrasting sources and processes of particulate species in haze days
628 with low and high relative humidity in wintertime Beijing, *Atmos. Chem. Phys.*, 20, 9101–
629 9114, <https://doi.org/10.5194/acp-20-9101-2020>, 2020.
- 630 Jimenez, J. L., Jayne, J. T., Shi, Q., Kolb, C. E., Worsnop, D. R., Yourshaw, I., Seinfeld, J. H.,
631 Flagan, R. C., Zhang, X., Smith, K. A., Morris, J. W., and Davidovits, P.: Ambient aerosol
632 sampling using the Aerodyne aerosol mass spectrometer, *J. Geophys. Res. Atmos.*, 108, 1–
633 13, <https://doi.org/10.1029/2001jd001213>, 2003.
- 634 Jimenez, J. L., Canagaratna, M. R., Donahue, N. M., Prevot, A. S. H., Zhang, Q., Kroll, J. H.,
635 DeCarlo, P. F., Allan, J. D., Coe, H., Ng, N. L., Aiken, A. C., Docherty, K. S., Ulbrich, I.
636 M., Grieshop, A. P., Robinson, A. L., Duplissy, J., Smith, J. D., Wilson, K. R., Lanz, V. A.,
637 Hueglin, C., Sun, Y. L., Tian, J., Laaksonen, A., Raatikainen, T., Rautiainen, J., Vaattovaara,
638 P., Ehn, M., Kulmala, M., Tomlinson, J. M., Collins, D. R., Cubison, M. J., Dunlea, E. J.,
639 Huffman, J. A., Onasch, T. B., Alfarra, M. R., Williams, P. I., Bower, K., Kondo, Y.,
640 Schneider, J., Drewnick, F., Borrmann, S., Weimer, S., Demerjian, K., Salcedo, D., Cottrell,
641 L., Griffin, R., Takami, A., Miyoshi, T., Hatakeyama, S., Shimono, A., Sun, J. Y., Zhang,
642 Y. M., Dzepina, K., Kimmel, J. R., Sueper, D., Jayne, J. T., Herndon, S. C., Trimborn, A.
643 M., Williams, L. R., Wood, E. C., Middlebrook, A. M., Kolb, C. E., Baltensperger, U., and
644 Worsnop, D. R.: Evolution of organic aerosols in the atmosphere, *Science (80-.)*, 326,
645 1525–1529, <https://doi.org/10.1126/science.1180353>, 2009.
- 646 Kuang, Y., He, Y., Xu, W., Yuan, B., Zhang, G., Ma, Z., Wu, C., Wang, C., Wang, S., Zhang,
647 S., Tao, J., Ma, N., Su, H., Cheng, Y., Shao, M., and Sun, Y.: Photochemical Aqueous-Phase
648 Reactions Induce Rapid Daytime Formation of Oxygenated Organic Aerosol on the North
649 China Plain, *Environ. Sci. Technol.*, 54, 3849–3860,
650 <https://doi.org/10.1021/acs.est.9b06836>, 2020.
- 651 Lee, A. K. Y., Chen, C. L., Liu, J., Price, D. J., Betha, R., Russell, L. M., Zhang, X., and Cappa,
652 C. D.: Formation of secondary organic aerosol coating on black carbon particles near
653 vehicular emissions, *Atmos. Chem. Phys.*, 17, 15055–15067, <https://doi.org/10.5194/acp-17-15055-2017>, 2017.
- 655 Li, H., Zhang, Q., Zhang, Q., Chen, C., Wang, L., Wei, Z., Zhou, S., Parworth, C., Zheng, B.,
656 Canonaco, F., Prévôt, A. S. H., Chen, P., Zhang, H., Wallington, T. J., and He, K.:
657 Wintertime aerosol chemistry and haze evolution in an extremely polluted city of the North
658 China Plain: Significant contribution from coal and biomass combustion, *Atmos. Chem.
659 Phys.*, 17, 4751–4768, <https://doi.org/10.5194/acp-17-4751-2017>, 2017.

660 Li, J., Liu, Z., Gao, W., Tang, G., Hu, B., Ma, Z., and Wang, Y.: Insight into the formation and
661 evolution of secondary organic aerosol in the megacity of Beijing, China, *Atmos. Environ.*,
662 220, <https://doi.org/10.1016/j.atmosenv.2019.117070>, 2020.

663 Middlebrook, A. M., Bahreini, R., Jimenez, J. L., and Canagaratna, M. R.: Evaluation of
664 composition-dependent collection efficiencies for the Aerodyne aerosol mass spectrometer
665 using field data, *Aerosol Sci. Technol.*, 46, 258–271,
666 <https://doi.org/10.1080/02786826.2011.620041>, 2012.

667 Ng, N. L., Canagaratna, M. R., Zhang, Q., Jimenez, J. L., Tian, J., Ulbrich, I. M., Kroll, J. H.,
668 Docherty, K. S., Chhabra, P. S., Bahreini, R., Murphy, S. M., Seinfeld, J. H., Hildebrandt,
669 L., Donahue, N. M., Decarlo, P. F., Lanz, V. A., Prévôt, A. S. H., Dinar, E., Rudich, Y., and
670 Worsnop, D. R.: Organic aerosol components observed in Northern Hemispheric datasets
671 from Aerosol Mass Spectrometry, *Atmos. Chem. Phys.*, 10, 4625–4641,
672 <https://doi.org/10.5194/acp-10-4625-2010>, 2010.

673 Ng, N. L., Canagaratna, M. R., Jimenez, J. L., Chhabra, P. S., Seinfeld, J. H., and Worsnop, D.
674 R.: Changes in organic aerosol composition with aging inferred from aerosol mass spectra,
675 *Atmos. Chem. Phys.*, 11, 6465–6474, <https://doi.org/10.5194/acp-11-6465-2011>, 2011.

676 Onasch, T. B., Trimborn, A., Fortner, E. C., Jayne, J. T., Kok, G. L., Williams, L. R., Davidovits,
677 P., and Worsnop, D. R.: Soot particle aerosol mass spectrometer: Development, validation,
678 and initial application, *Aerosol Sci. Technol.*, 46, 804–817,
679 <https://doi.org/10.1080/02786826.2012.663948>, 2012.

680 Paatero, P.: The Multilinear Engine—A Table-Driven, Least Squares Program for Solving
681 Multilinear Problems, Including the n-Way Parallel Factor Analysis Model, *J. Comput.*
682 *Graph. Stat.*, 8, 854–888, <https://doi.org/10.1080/10618600.1999.10474853>, 1999.

683 Sullivan, A. P., Hodas, N., Turpin, B. J., Skog, K., Keutsch, F. N., Gilardoni, S., Paglione, M.,
684 Rinaldi, M., Decesari, S., Cristina Facchini, M., Poulain, L., Herrmann, H., Wiedensohler,
685 A., Nemitz, E., Twigg, M., and Collett, J. L.: Evidence for ambient dark aqueous SOA
686 formation in the Po Valley, Italy, *Atmos. Chem. Phys.*, 16, 8095–8108,
687 <https://doi.org/10.5194/acp-16-8095-2016>, 2016.

688 Su, J., Zhao, P., Ge, S., and Ding, J.: Aerosol liquid water content of PM_{2.5} and its influencing
689 factors in Beijing, China, *Sci. Total Environ.*, 839, 156342,
690 <https://doi.org/10.1016/j.scitotenv.2022.156342>, 2022.

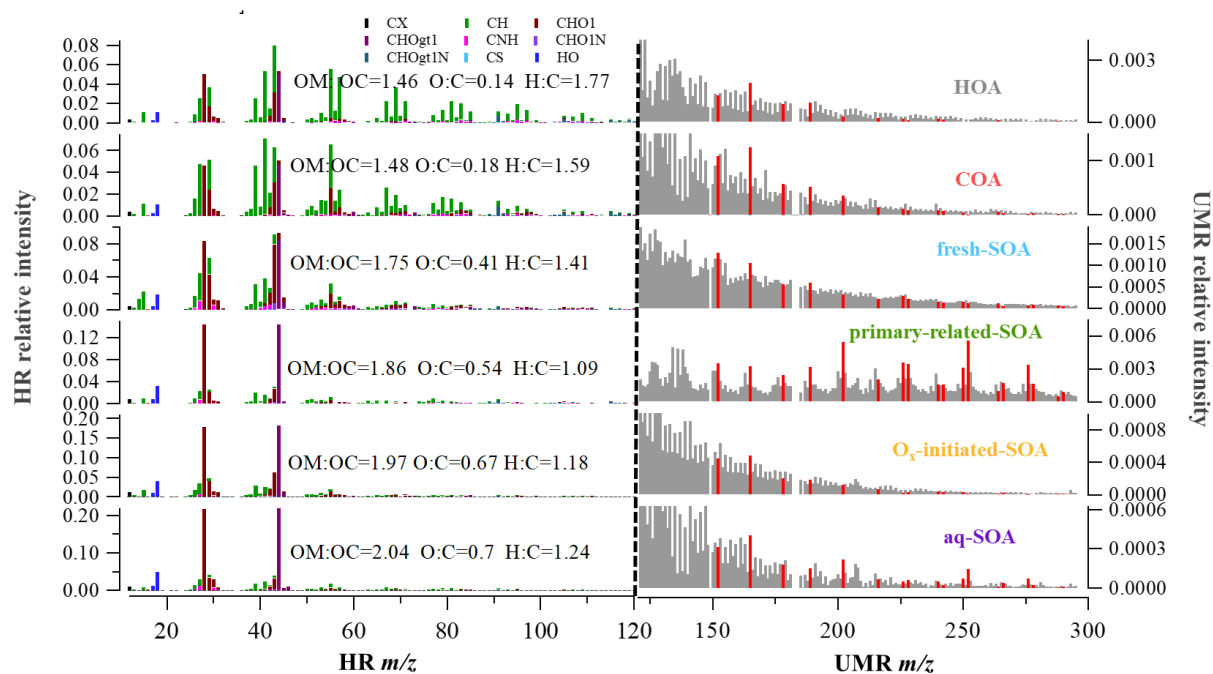
691 Sun, Y., Chen, C., Zhang, Y., Xu, W., Zhou, L., Cheng, X., Zheng, H., Ji, D., Li, J., Tang, X.,
692 Fu, P., and Wang, Z.: Rapid formation and evolution of an extreme haze episode in Northern
693 China during winter 2015, 1–9, <https://doi.org/10.1038/srep27151>, 2016.

694 Sun, Y., Xu, W., Zhang, Q., Jiang, Q., Canonaco, F., Prévôt, A. S. H., Fu, P., Li, J., Jayne, J.,
695 Worsnop, D. R., and Wang, Z.: Source apportionment of organic aerosol from 2-year highly
696 time-resolved measurements by an aerosol chemical speciation monitor in Beijing, China,
697 *Atmos. Chem. Phys.*, 18, 8469–8489, <https://doi.org/10.5194/acp-18-8469-2018>, 2018a.

- 698 Sun, Y., Xu, W., Zhang, Q., Jiang, Q., Canonaco, F., and Prévôt, A. S. H.: Source
699 apportionment of organic aerosol from two-year highly time- resolved measurements by an
700 aerosol chemical speciation monitor in Beijing , China, 2018b.
- 701 Sun, Y. L., Zhang, Q., Anastasio, C., and Sun, J.: Insights into secondary organic aerosol
702 formed via aqueous-phase reactions of phenolic compounds based on high resolution mass
703 spectrometry, *Atmos. Chem. Phys.*, 10, 4809–4822, [https://doi.org/10.5194/acp-10-4809-](https://doi.org/10.5194/acp-10-4809-2010)
704 2010, 2010.
- 705 Wang, J., Ye, J., Zhang, Q., Zhao, J., Wu, Y., Li, J., Liu, D., Li, W., Zhang, Y., Wu, C., Xie,
706 C., Qin, Y., Lei, Y., Huang, X., Guo, J., Liu, P., Fu, P., Li, Y., Lee, H. C., Choi, H., Zhang,
707 J., Liao, H., Chen, M., Sun, Y., Ge, X., Martin, S. T., and Jacob, D. J.: Aqueous production
708 of secondary organic aerosol from fossil-fuel emissions in winter Beijing haze, *Proc. Natl.*
709 *Acad. Sci. U. S. A.*, 118, 1–6, <https://doi.org/10.1073/pnas.2022179118>, 2021.
- 710 Wang, S., Newland, M. J., Deng, W., Rickard, A. R., Hamilton, J. F., Muñoz, A., Ródenas, M.,
711 Vázquez, M. M., Wang, L., and Wang, X.: Aromatic Photo-oxidation, A New Source of
712 Atmospheric Acidity, *Environ. Sci. Technol.*, 54, 7798–7806,
713 <https://doi.org/10.1021/acs.est.0c00526>, 2020.
- 714 Xu, S., Liu, W., and Tao, S.: Emission of Polycyclic Aromatic Hydrocarbons in China,
715 *Biophys. Process. Anthropol. Org. Compd. Environ. Syst.*, 40, 267–281,
716 <https://doi.org/10.1002/9780470944479.ch11>, 2006.
- 717 Xu, W., Han, T., Du, W., Wang, Q., Chen, C., Zhao, J., Li, J., Fu, P., Wang, Z., Worsnop, D.
718 R., and Sun, Y.: Effects of Aqueous-phase and Photochemical Processing on Secondary
719 Organic Aerosol Formation and Evolution in Beijing , China,
720 <https://doi.org/10.1021/acs.est.6b04498>, 2017.
- 721 Xu, W., Sun, Y., Wang, Q., Zhao, J., Wang, J., Ge, X., Xie, C., Zhou, W., Du, W., Li, J., Fu,
722 P., Wang, Z., Worsnop, D. R., and Coe, H.: Changes in Aerosol Chemistry From 2014 to
723 2016 in Winter in Beijing: Insights From High-Resolution Aerosol Mass Spectrometry, *J.*
724 *Geophys. Res. Atmos.*, 124, 1132–1147, <https://doi.org/10.1029/2018JD029245>, 2019.
- 725 Ye, C., Liu, P., Ma, Z., Xue, C., Zhang, C., Zhang, Y., Liu, J., Liu, C., Sun, X., and Mu, Y.:
726 High H₂O₂ Concentrations Observed during Haze Periods during the Winter in Beijing:
727 Importance of H₂O₂ Oxidation in Sulfate Formation, *Environ. Sci. Technol. Lett.*, 5, 757–
728 763, <https://doi.org/10.1021/acs.estlett.8b00579>, 2018.
- 729 Zhang, Q., Jimenez, J. L., Canagaratna, M. R., Ulbrich, I. M., Ng, N. L., Worsnop, D. R., and
730 Sun, Y.: Understanding atmospheric organic aerosols via factor analysis of aerosol mass
731 spectrometry: A review, <https://doi.org/10.1007/s00216-011-5355-y>, 2011.
- 732 Zhao, J., Qiu, Y., Zhou, W., Xu, W., Wang, J., Zhang, Y., Li, L., Xie, C., Wang, Q., Du, W.,
733 Worsnop, D. R., Canagaratna, M. R., Zhou, L., Ge, X., Fu, P., Li, J., Wang, Z., Donahue, N.
734 M., and Sun, Y.: Organic Aerosol Processing During Winter Severe Haze Episodes in
735 Beijing, *J. Geophys. Res. Atmos.*, 124, 10248–10263,
736 <https://doi.org/10.1029/2019JD030832>, 2019.

737

738 **Figures**

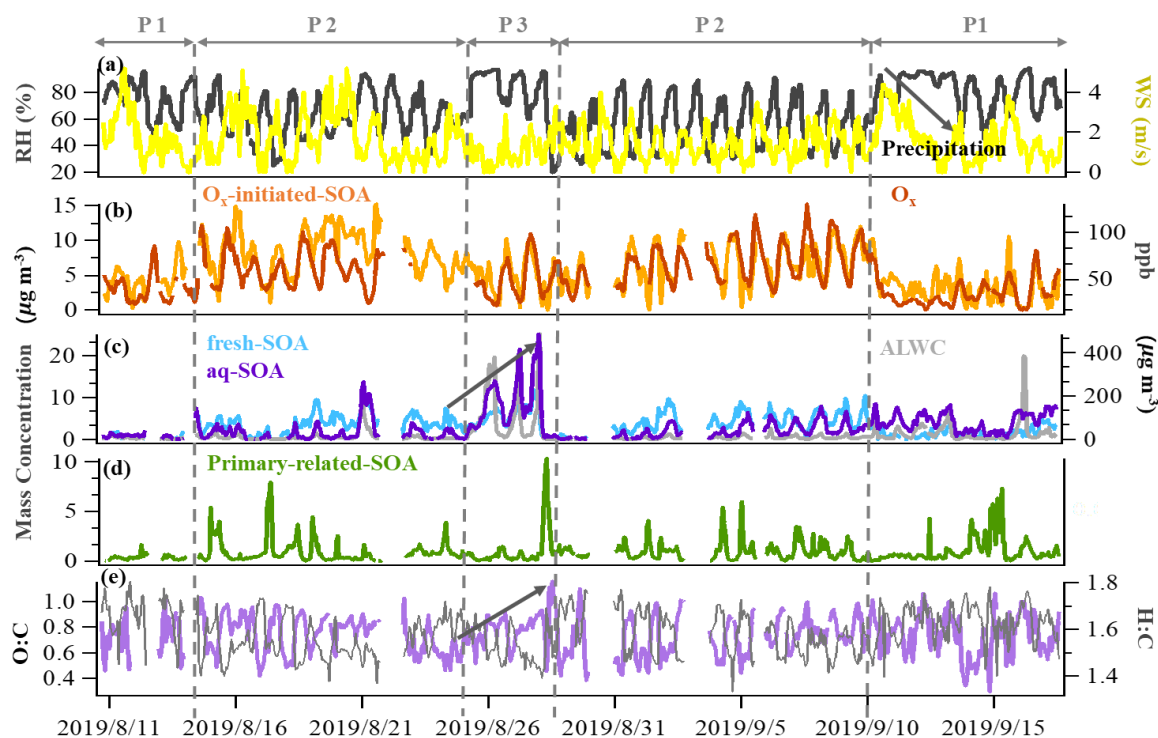


739

740 **Fig. 1** HR and UMR mass spectra of OA factors: (a) HOA; (b) COA; (c) fresh-SOA; (d)
741 primary-related-SOA; (e) O_x-initiated-SOA; (f) aq-SOA. Mass spectra signals less than 120
742 amu are colored by nine ion categories, signals equal to or greater than 120 amu are in unit
743 mass resolution, and polycyclic aromatic hydrocarbons (PAHs) signals are in red on the right
744 panels.

745

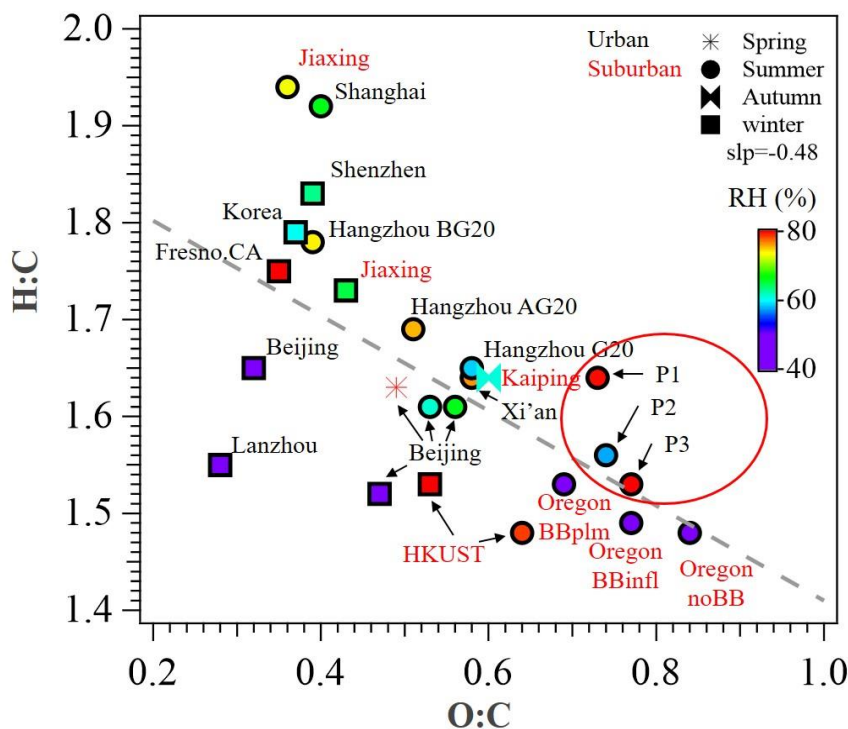
746



747

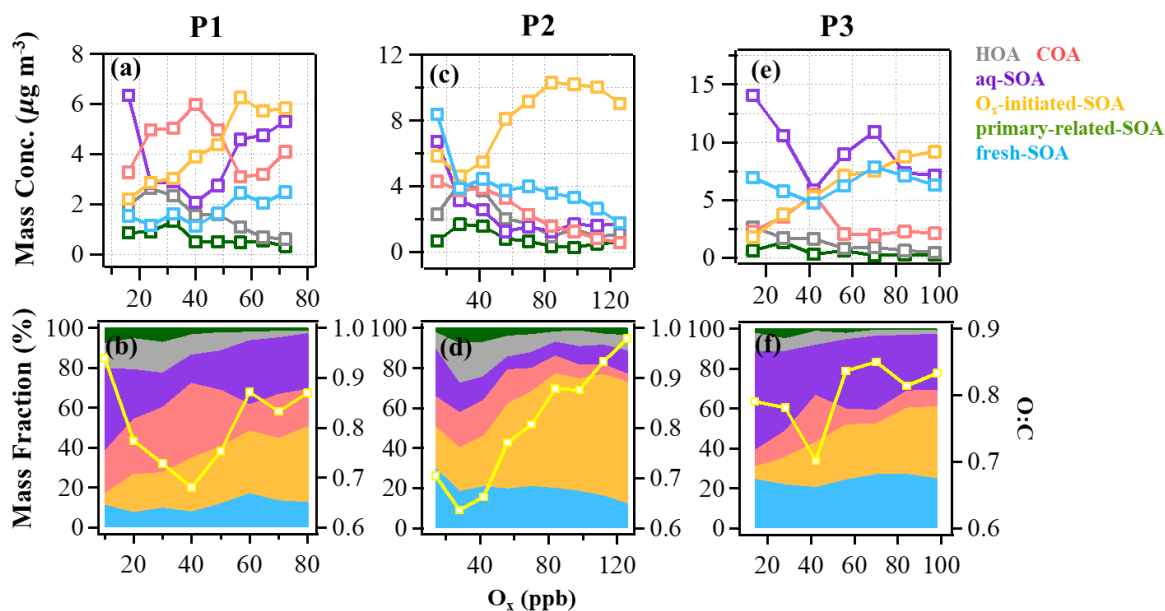
748 **Fig. 2** Time series of (a) relative humidity (RH) and wind speed (WS), (b) O_x and O_x-initiated-
 749 SOA, (c) fresh-SOA, aq-SOA and ALWC, (d) primary-related-SOA, (e) the O:C ratio and H:C
 750 ratio. The time series were categorized to be three typical periods based on total SOA mass
 751 concentrations and meteorology conditions: reference period (P1), high O_x period (P2) and high
 752 RH period (P3).

753



754

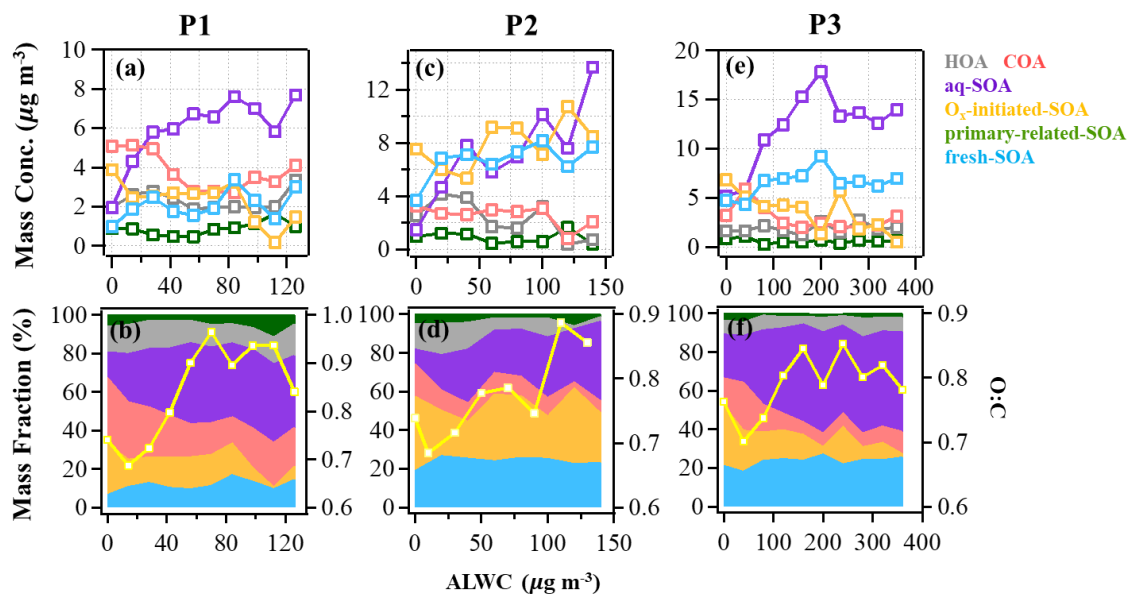
755 **Fig.3** Van Krevelen plot for OA of urban and suburban sites in China and other nations. Data
 756 points are colored by RH (%). P1, P2 and P3 in red circles represents the different periods in
 757 this study. All the data and related references can be found in Table S3.



758

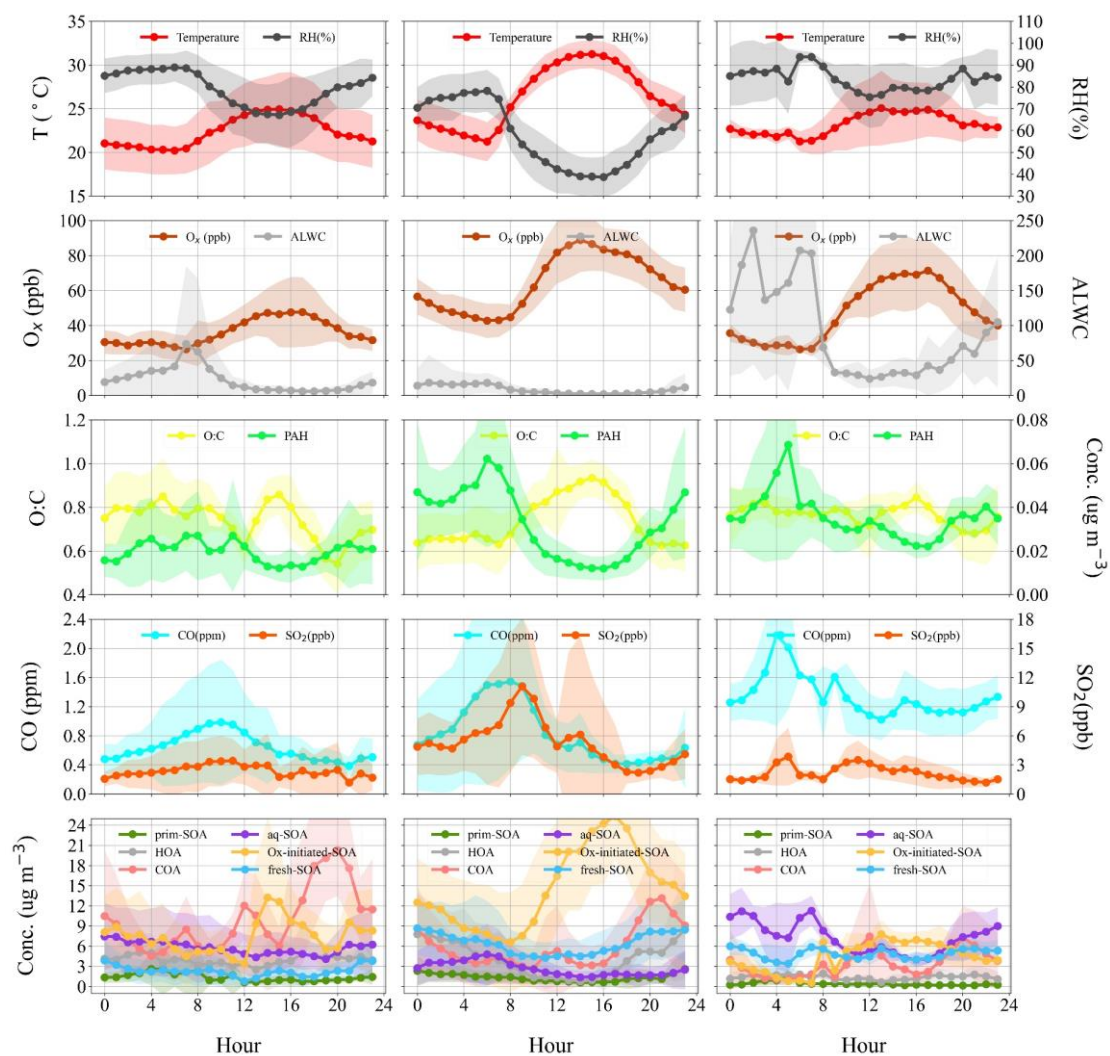
759 **Fig. 4** The mass concentration and contribution of OA factors as functions of O_x in reference
 760 period (P1: a & b), high O_x period (P2: c & d) and high RH period (P3: e & f) during this

761 campaign. The yellow curves represent the O:C ratio vs. O_x . The data were binned according
 762 to O_x concentration (10 ppb increment in P1, 14 ppb increment in P2 and P3).



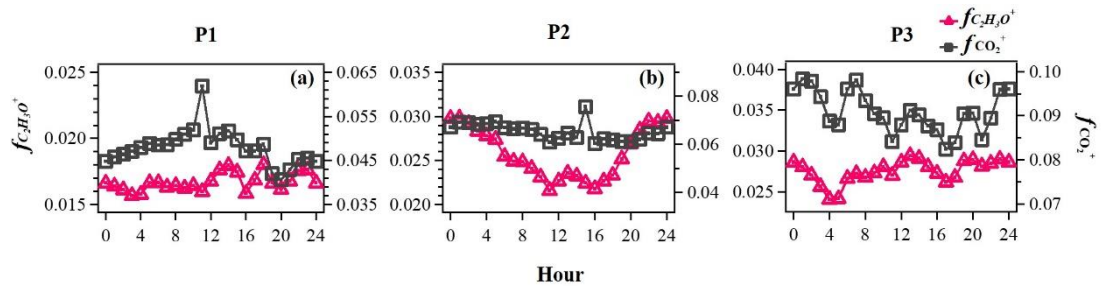
763

764 **Fig. 5** The mass concentration and contribution of OA factors as functions of ALWC in
 765 reference period (P1: a & b), high O_x period (P2: c & d) and high RH period (P3: e & f) during
 766 this campaign. The yellow curves represent the O:C ratio v.s. ALWC. The data were binned
 767 according to the ALWC concentration ($14 \mu\text{g m}^{-3}$, $20 \mu\text{g m}^{-3}$ and $40 \mu\text{g m}^{-3}$ increment in P1 P2
 768 and in P3).



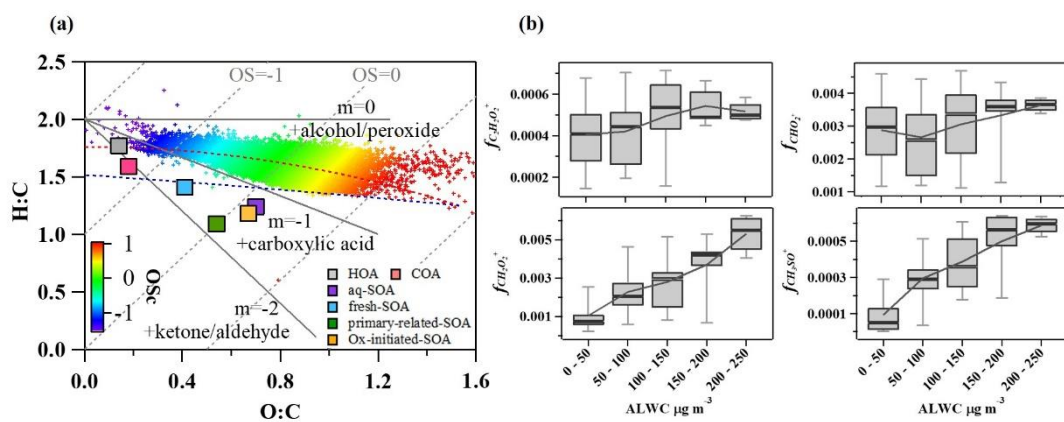
769

770 **Fig. 6** Diurnal patterns of meteorological parameters (T, RH), gaseous species (O_x, CO, SO₂),
 771 ALWC (liquid water content), O:C (oxygen-to-carbon elemental ratio), polycyclic aromatic
 772 hydrocarbons (PAHs) fragments and OA factors in reference period (P1), high O_x period (P2)
 773 and high RH period (P3) in this campaign.



774

775 **Fig. 7** Evolution of high-resolution organic mass spectra on changes in relative intensities (mass
 776 fraction) of oxygen-containing ions: $C_2H_3O^+$ (m/z 43) and CO_2^+ (m/z 44) in reference period
 777 (P1: a), high O_x period (P2: b) and high RH period (P3: c) in this campaign.



778

779 **Fig. 8** (a) Van Krevelen diagram for the O:C and H:C ratios of different OA factors (marked
 780 with squares) and bulk of OA during summer (marked with plus signs and colored by
 781 Oscarbon oxidation state (OSc)); (b) Mass fractions of ion fragments indicative of aqueous-
 782 phase processing and oxygenated functional groups (alcohols, carboxylic acids) as a function
 783 of ALWC.